Network modelling analysis of a depressurization experiment on a North Sea reservoir core sample

Network Modelling Analysis of a Depressurization Experiment on a North Sea Reservoir Core Sample

[1]Bagudu, U., [2]McDougall, S. R., and [2]Mackay, E. J.
[1]National Grid Gas, Warwick, UK; [2]Institute of Petroleum Engineering, Heriot-Watt University, Edinburgh, UK.

Keywords: Network modelling, Solution gas drive, crtical gas saturation, depressurization, depletion rate

[1]**Corresponding author**: usman.bagudu@nationalgrid.com; +44 (0)7774269483

Abstract
Solution gas drive following depressurization of oil reservoirs below the bubble point is the oldest and perhaps one of the most challenging oil recovery mechanisms to quantify. Part of the challenge lies in designing repeatable experiments and then translating experimental observations into practical solutions in the field – laboratory depressurisation rates are typically orders of magnitude higher than practical field rates. Using a case study we show how pore network modelling can help make sense of the underlying physical mechanisms governing gas flow behaviour in porous media during solution gas drive whilst also serving as a forward modelling tool for developing relative permeability functions for use in field scale simulators. Core scale simulations performed on a pore network anchored to measured petrophysical properties of a 0.23mD chalk core from a North Sea reservoir show a very weak correlation between depletion rate and critical gas saturation, contrary to observations in higher permeability clastic media. In addition, solution gas drive oil recovery was found to increase with higher initial water saturation.

1 Introduction

1.1 General context

Solution gas drive was one of the first petroleum production techniques to be implemented in the field, essentially due to its simplicity of application — the energy required for oil displacement being provided cheaply through gas and liquid expansion as a consequence of continuous fluid withdrawal from the reservoir. Gas dissolved in the oil is progressively liberated from solution, expands in place and subsequently migrates towards low pressure regions (i.e. towards regions of higher elevation within the reservoir due to hydrostatic forces and towards regions around production wells). During volume expansion of the gaseous phase, equivalent volumes of oil are expelled from the pore space resulting in oil flow towards the producers. For an undersaturated reservoir undergoing solution gas drive, three different stages can be identified:

1. ***Liquid expansion:*** oil is displaced from the reservoir through liquid expansion. Reservoir pressure falls quickly due to the low compressibility of the oil
2. ***Gas liberation:*** when pressure falls below a certain critical value (known as the *bubble point pressure*), the reservoir becomes a *gas*-saturated oil reservoir, gas is liberated from solution in the form of small gas bubbles and the oil phase begins to shrink. At this point oil production rates generally decrease, since the evolving gas saturation partially fills the host porous medium, thereby decreasing the relative permeability to oil.
3. ***Continuous gas flow:*** eventually the gas saturation increases to such an extent that isolated gas clusters become connected to one another and continuous gas flow begins — the minimum gas saturation at which this occurs is commonly referred to as the "critical gas saturation". During this latter phase, produced gas-oil ratios tend to increase monotonically and oil productivity continues to decline.

Solution-gas drive is generally characterised by a rapid pressure decline and low recovery efficiency and, for this reason, more efficient recovery techniques, such as waterflooding and gasflooding have often been used. Nevertheless, the process of solution gas drive finds renewed interest in many areas of the world under the guise of "reservoir depressurisation": technological advances coupled with diminishing reserves mean that solution gas drive techniques are becoming economically attractive for a range of both virgin and waterflooded reservoirs. Extensive applications to the former are found in heavy oil recovery (sometimes under the name of cold heavy oil production) especially in Western Canada and Venezuela (De Mirabal et al. (1997), Lago et al. (2002)). For waterflooded reservoirs, the technique provides a valuable approach to appreciably extend the life of a reservoir that has undergone waterflooding for many years (Ligthelm et al. (1997), Goodfield et al. (2003), Petersen et al. (2004), Boge et al. (2005), Bratvold and Thomas (2015)).

Unfortunately, productivity forecasts for solution gas drive are not easily undertaken. The main reason lies in the uncertain determination of the initial reservoir properties (at bubble point pressure), together with our (still) relatively limited understanding of the related physico-chemical mechanisms that take place at the pore scale. Such an understanding is fundamental for generating appropriate input data for use in reservoir simulation studies which, in turn, facilitate efficient and reliable depressurisation management.

Previous published works have covered topics ranging from the build-up of supersaturation and related nucleation of embryonic bubbles, to the growth of the gaseous phase, the study of critical gas saturations and the regimes of gas flow. There is a rich catalogue of experimental techniques; from the first attempts utilising simple methane and kerosene mixtures in the presence of calcite and silica crystals (Kennedy and Olson, 1952) to laboratory core tests (Handy, 1958; Firoozabadi et al., 1992; Scherpenisse et al., 1994; Akin and Kovscek, 2002; Piccavet et al., 2006; Alshmakhy, A. and Maini, B., 2012) and visualization methods using glass-etched micromodels (El Yousfi et al., 1997; Mackay et al., 1998; Bora et al., 2000; Nejad and Danesh, 2005). In addition, a number of different theoretical models for gas phase evolution have been proposed (Moulu and Longeron, 1989; Firoozabadi and Kashiev, 1993; Li and Yortsos, 1993; Tsimpanogiannis and Yortsos, 2002).

Despite this abundance of studies, however, it still appears that no generally accepted theory for gas evolution in porous media has yet been agreed upon; nor has any generalised procedure for estimating critical gas saturation been developed. The conclusion seems to be that gas evolution during solution gas drive depends strongly upon both the experimental set-up under consideration and the subtle interaction between the corresponding rock and fluid properties.

1.2 Motivation

Pore network modelling has shown great potential as a tool for gaining valuable insight into complex experimental situations because of it's ability to explicitly represent physical phenomena at a fundamental scale. It is therefore uniquely suited for investigating the complex interplay of the physico-chemical processes during reservoir depressurization below bubble point. Such a process simulator has been developed (McDougall and Mackay, 1998; Bondino et al., 2005; Ezeuko et al., 2010) and has continued to be refined and extended (Bagudu, 2015).

As a result of experimental data recently becoming available from the North Sea, an opportunity has been presented for a detailed investigation of a number of important issues pertaining to pressure depletion in waterflooded chalk. By incorporating experimentally-determined core and fluid data, the process simulator can initially be used to interpret depressurisation experiments and subsequently utilised to predict low-rate depletion behaviour over a range of length-scales: from the plug scale to the large core scale. In addition, several different boundary conditions can be considered and any inconsistencies reconciled.

Field A [*a pseudonym*] is a fractured chalk reservoir situated in the Central Graben of the UKCS and has historically been produced via voidage replacement water injection. However, following a few years of injection, an unexpectedly high water-cut has been observed and this has led the field management team to consider a range of revised development plans. The current viewpoint is that water injection into the chalk matrix should be continued until the water cut becomes unacceptable, at which point a depressurisation strategy should be invoked in order to displace additional oil. Unfortunately, supporting evidence for the strategy is somewhat lacking at present and it is not possible to carry out an isolated pilot depletion in the field to assess its potential.

In order to address this deficiency and provide some background data for associated simulation studies, a moderate-rate, post-waterflood depletion experiment has been completed. Analysis of the measurements suggests a significant decrease in residual oil saturation from approximately 38% to 18% after depressurisation – surprisingly, no significant water production was observed during the experiment. However, a number of uncertainties remain with regard to the relevance of the experimental results to the field: (i) the laboratory depletion rate significantly exceeded that practically achievable in the field; (ii) production was restricted to the top of the sample, raising the possibility that buoyancy effects could have biased the results; and (iii) constant composition expansion was assumed to be a suitable model for assessing oil shrinkage but this may not be appropriate.

1.3 Objectives and paper outline

The main objectives of this case study are:

I. To anchor the pore-scale simulator to reservoir samples using petrophysical data obtained in the laboratory.
II. To build a numerical model of the reservoir sample by matching the experimental production profiles.
III. To undertake a parametric study of the depressurisation process at the pore-scale, using the pore network model as an investigative tool to offer an interpretation of the experimental trends.
IV. To use this numerical surrogate to examine production and relative permeability issues using different depletion rates and different rock/fluid parameters; and
V. To use the simulation results to re-interpret a range of experimental data and help explain any apparent inconsistencies

Because of the direct relevance of the results to field operations, field units will be used throughout this paper.

2 Model Setup

2.1 The Basic Model

The basic network model is a three dimensional lattice of interconnected capillary elements with a coordination number of 6 (Figure 1). Less well-connected network topologies can be modelled by removing elements at random. Single phase flow through the network is modelled by applying Poiseuille-like flow across each pore element and then invoking conservation of mass at the intersection of pore elements (nodes) which yields a set of linear equations that can be solved for pressures at each node. The simplest two-phase flow is modelled as an invasion percolation either by drainage or imbibition. The model allows for hydraulic trapping of both wetting and non-wetting phases (McDougall & Sorbie, 1997).

2.2 Network Anchoring

The appeal of lattice network models lies in the ease with which they can be lithologically 'anchored' to cheap, accessible experimental data using only a handle of parameters and then subsequently used to make predictions of petrophysical properties such as capillary pressures and gas/oil relative permeabilities.

Although developments in pore-scale imaging and reconstruction techniques have produced *in silico* models that appear – at least visually – to be direct numerical analogues of the parent sample, the ability of such models to make *a priori* predictions has recently been called into question (McDougall and Sorbie, 2002; Bondino et al., 2009; Sorbie and Skauge, 2011; Bondino et al, 2012). Moreover, reconstruction protocols require extensive CPU capacities and are consequently limited to producing relatively small 3D networks – systems that are often inadequate for assessing crucial force balances that operate at larger scales. In order to overcome such shortcomings, it is often preferable to utilise more primitive models that, although lacking the fine geometrical detail found in reconstructed pore systems, can include all of the pertinent physics at the appropriate scale. This is particularly true in the present situation, where core-scale laboratory experiments are to be interpreted with respect to capillary and gravitational forces.

The network anchoring approach used here is after McDougall et al (2002) and involves matching mercury injection capillary pressure (MICP) data from experiments to extract pore size distribution and pore volume scaling information. The anchoring method takes advantage of the stable structure exhibited by the inverse capillary pressure plots i.e. R vs SHg ($R=2\sigma\cos\theta/P_c$)to facilitate the matching. The anchoring method is modelled on the "3Rs" network model framework in which each pore element is assigned a capillary radius, a volume and a conductance, with the following functional dependencies.

$$\begin{aligned} Pc &\propto 1/r \\ v(r) &\propto r^{v} \\ g(r) &\propto r^{\lambda} \end{aligned} \qquad (1)$$

where *Pc* is the capillary pressure, *v(r)* is the pore volume, and *g(r)* the pore conductivity as a function of capillary entry radius, *r*.

The shape of the R-plot is determined by the analytical equation

$$S_{Hg}(r) = A(r) {S_{Hg}}^{A\equiv 1}(r) \qquad (2)$$

where $S_{Hg}(r)$ is the mercury saturation at percolation radius r. $A(r)$ is the accessibility function defined as the ratio of the number of invaded pores to the number that would have been invaded if each pore had a direct connection to the inlet; ${S_{Hg}}^{A\equiv 1}(r)$ is the saturation at perfect accessibility and is given as

$$S_{Hg}(r) = \int_{r}^{r_{max}} v(r) f(r) dr = \frac{r_{max}^{v+n+1} - r^{v+n+1}}{r_{max}^{v+n+1} - r_{min}^{v+n+1}} \qquad (3)$$

Where $f(r)$ is the pore size distribution component which also has a power law dependence as $f(r) \propto r^{n}$, where $n < 0$ $(n > 0)$.

McDougall et (2002) derived an analytic form of the accessibility function, $A(r)$, as a function of the network size and the coordination number via,

$$A(p) = \frac{1}{1+10^{4}\exp(-6.14zp)} \qquad (4)$$

where z is the coordination number and p is the number fraction of pores that would have been invaded for the fully accessible case. The accessibility function expressed in terms of pore radius yields

$$A(r) = \frac{1}{1+10^4 \exp\left[-6.14z\left(\frac{r_{max}^{n+1} - r^{n+1}}{r_{max}^{n+1} - r_{min}^{n+1}}\right)\right]} \quad (5)$$

Using equations (2) to (5) a best fit analytical R-plot to the experimental data was generated by adjusting the range of pore radius (r_{max}, r_{min}); the pore volume exponent (v); the pore size distribution exponent (n); and the coordination number (z). These constrained set of adjustable parameters define the pore size distribution, pore volume scaling and topological information for the network model.

Figure 2 compares the experimental R-plot with analytical plots generated from a set of matching parameters. The R-plots from network simulations which used the matching parameters as inputs have also been overlaid on the graph for comparison.

Figure 3 compares the experimental curve with simulated drainage curves at different random seeds, this time expressed in terms of capillary pressure vs. water saturation. The apparent lack of variation across the three random seeds indicates a sufficiently large number of pores in the network (25x25x25) to smooth out the effects of any localised heterogeneities on the overall network saturation.

Capillary pressure gradient plots – generally derived from porosimetry data and sometimes (incorrectly) reported as pore size distribution functions – are presented for both the experiment and simulation in Figure 4. In Figure 4

$$D(r) = \frac{P_c}{r}\left(\frac{dS_{Hg}}{dP_c}\right) \quad (6)$$

Where $D(r)$ is the so called "pore size distribution" but which on closer analysis was found to be a pore volume-weighted distribution (McDougall, 1994). Equation (6) was first introduced by Ritter and Drake (1945).

The PDF plot of the generated network radii (Figure 5) suggests a relatively uniform (i.e. flat) pore size distribution.

2.3 The Solution Gas Drive Model

The pore scale physics at each step of the solution gas drive process was modelled explicitly. Starting from the nucleation of an embryonic bubble upon the system falling below the bubble point to the diffusion of solution gas into the bubble and the subsequent growth of bubble under the influence of capillary, gravity and viscous forces. The precise details of the modelling can be found in Chapter 3 of Bagudu (2015). Here we present a summary of the pertinent process steps.

2.3.1 Bubble Nucleation*:*

The nucleation model is the pre-existing vapour model (after Yortsos and Parlar, 1989). Assuming a pre-existing gas bubble, a crevice of radius W is assumed to be activated when the local supersaturation exceeds the capillary threshold of the crevice, *viz*:

$$(KC - P_l) \geq \frac{2\sigma cos\theta}{W} \quad (7)$$

where K is the gas solubility constant, C the local dissolved gas concentration, P_l the local liquid pressure, σ is the gas/liquid interfacial tension and θ is the contact angle.

2.3.2 Mass Diffusion*:*

A first-principles multiphase diffusion model has been incorporated that allows for different gas/oil and gas/water diffusion coefficients to be considered. Multiphase concentration gradients are calculated throughout the depletion as they dynamically evolve.

The dissolved gas concentration at the gas/oil or gas/water interface is assumed to instantaneously reach an equilibrium value that is determined by the current system pressure. A dissolved gas concentration gradient is thus set up which drives dissolved gas towards the embryonic bubble that acts as a gas sink. The mass flux across unit cross-sectional area in unit time from pore i to pore j is given by Fick's first law:

$$\boldsymbol{J_{ij} = -D(C_j - C_i)/L} \tag{8}$$

where C_i the gas concentration in pore i, C_j the gas concentration in pore j, D the diffusion coefficient, and L a diffusion length (taken here to be equal to the distance between two pore centres).

Mass flux across an oil-filled or water filled pore will change its concentration and this time evolution of concentration is evaluated by discretizing Fick's second law,

$$\boldsymbol{\frac{\partial C}{\partial t} = \frac{\partial}{\partial x}\left(D\,\frac{\partial C}{\partial x}\right)} \tag{9}$$

to the form

$$\boldsymbol{C_i^{new} = C_i^{old} + \Delta t\left[\frac{mass\ in - mass\ out}{Vi}\right] = \frac{\Delta m_i(\Delta t)}{Vi}} \tag{10}$$

where Vi is the pore volume and Δt the time step.

For pore i, the area-weighted sum of diffusion fluxes $\Delta m_i(\Delta t)$, is given as

$$\boldsymbol{\Delta m_i(\Delta t) = \sum_{n=1}^{6} J_i \times \mathbf{min}(A_n,\ A_i)} \tag{11}$$

where A is the pore cross-sectional area and n an index running through all perimeter pores.

The $\mathbf{min}$ term in Equation (11) means that mass diffusion is constrained by the minimum cross-sectional area between pores, making the peculiar characteristics of porous media architecture (pore size distribution, coordination number) an important governing parameter of a depletion process.

2.3.3 Bubble Growth*:*

Bubble growth is followed from the embryonic stage through to the formation of a network spanning cluster. Pressure-dependent interfacial tensions (IFTs) and spreading coefficients are considered throughout bubble growth. Gas evolution in both virgin and waterflooded systems can be followed and double drainage events are also included (i.e. gas displacing oil followed by oil displacing water).
The bubble growth process is modeled in two stages in keeping with experimental observations of the depletion process in micromodels. The first stage involves the growth of the embryonic bubble within the host oil-filled pore as its pressure increases above the ambient pressure due to gas diffusing into it. In the second stage the bubble expands beyond its parent pore if its internal pressure is greater than the

minimum of the capillary entry thresholds of the oil-filled neighboring pores that are *not trapped* as expressed by Equation (12).

$$\boldsymbol{P_g > \ \min(P^i{}_c) + \ P_o} \tag{12}$$

i.e.

$$\boldsymbol{P_g - [\min(P^i{}_c) + \ P_o] = \min(\Delta P^i{}_c) > 0} \tag{13}$$

where, P_g = the absolute pressure of the gas phase = $Z(P,T)n(t)RT/V(t)$, n = current number of gas moles, R = universal gas constant, P = current pressure = P_o = the absolute pressure in the oil evaluated at the upper boundary of the network, T = current temperature, Z = gas compressibility factor, and $V(t)$ = current gas volume, $P^i{}_c$ = the static equilibrium capillary pressure in an available perimeter pore = $\eta\sigma cos\theta/r_i$, σ = interfacial tension, θ = gas-oil contact angle=0.0, r_i = pore radius, η = shape factor which is 2 for cylindrical pore elements, t the time, and i = an index running through all the available pores containing oil at the perimeter of the expanding gas.

If Equation (13) is not satisfied, the bubble is labeled as '*constrained*' and further growth is deferred so that the pressure of the bubble can continue to rise as new gas is added to it via diffusion whilst the interface is held in a quasi-static state.

The perturbative effect of gravity on bubble growth can be included in Equation (13) to give the pore invasion criteria around a cluster as

$$\boldsymbol{\min(\Delta P^i{}_c + \Delta P^i{}_h)^j > 0} \tag{14}$$

where,

$\Delta P^i{}_h = P^i{}_{h^o} - \ \Delta P^i{}_b$ is the net local gravity component

where,

$P^i{}_{h^o} = \rho_o g H^i$, stands for the local hydrostatic head due to the oil column. It increases with depth, i.e. bubbles at top of the network will grow faster than those at the bottom.

$\Delta P^i{}_b = \Delta\rho g h^{ij}$, stands for the local buoyancy pressure. It mainly controls the trajectory of bubble growth.

where H^i is the vertical distance between oil pore i and the top of the network, h^{ij} the vertical distance between oil pore i and the bottom of neighbouring gas cluster j, $\Delta\rho = \rho_o - \rho_g$, ρ_g the gas density, ρ_o the oil density, and g the gravitational acceleration.

The invasion criteria in Equation (14) can be further generalized to include the effect of an externally imposed pressure gradient as

$$\boldsymbol{\min(\Delta P^i{}_c + \Delta P^i{}_h + \Delta P^i{}_{vis})^j > 0} \tag{15}$$

were, $\Delta P^i{}_{vis}$ is the local viscous pressure gradient across an oil pore i at the perimeter of gas a cluster j and is calculated by invoking the mass conservation to calculate pressures at each node via a set of linear equations.

The viscous pressure component ($\boldsymbol{\Delta P^i{}_{vis}}$) is ignored in this study as the capillary number in a depressurization process in 'light oil' is assumed to be negligible. The bubble growth model just described thus reduces to the classic invasion percolation – the interface advances one pore at a time in discrete jumps equivalent to the length of a pore.

2.3.4 Buoyancy Module*:*

The effects of gravity upon gas evolution and migration have been captured in this module. Sensitivity studies have demonstrated that the precise physics governing the process of bubble migration contains a greater number of subtleties than previously thought (Dumore, 1970; Ezeuko, 2009).

As system scale increases gas bubbles could become sufficiently large as to spontaneously overcome the local capillary forces and thereby migrate up the system. Migration involves the activation of two displacement fronts simultaneously i.e. the drainage front at the top of the migrating bubble and the imbibition front mainly at the bottom of the bubble. Displacement at the drainage front is driven by

$$\Delta P^{i}{}_{Mig} = \Delta\rho g h^{ij} - \frac{2\sigma cos\theta}{r_i} \quad (16)$$

where all terms are as previously defined.

The imbibition process is modelled after the observations of Lenormand and Zarcone (1984, 1983). It is governed by local network topology as well as hydrostatic and capillary pressure considerations. The pressure difference required to spontaneously imbibe water or oil into a pore, i, filled with gas is given by the relation:

$$\Delta P^{i}_{imb} = \sigma / r^{i}[1.0 + \alpha^{i}] + \Delta P^{i}{}_{h} \quad (17)$$

where $\Delta P^{i}{}_{h}$ is as previously defined, and α is a topological parameter defined as

$$\boldsymbol{\alpha = max}\left[\boldsymbol{n_a^o}/(\boldsymbol{n_a^o} + \boldsymbol{n_a^g}),\ \boldsymbol{n_b^o}/(\boldsymbol{n_b^o} + \boldsymbol{n_b^g})\right] \quad (18)$$

where n^o and n^g represent the number of neighbouring pores on either sides (a and b) of pore *i* that are filled with oil.

2.3.5 Oil Shrinkage*:*

Oil shrinks as gas comes out of solution and the resulting void is filled with gas. Here oil is assumed to shrink preferentially from pores with the largest capillary entry radii since gas is more likely to invade these elements during expansion.

2.4 Network Dimensions

Building core-scale clastic network surrogates proves to be relatively straightforward and 2D models up to 1m in length have been reported (Ezeuko, 2009). However, Field A chalk pore sizes are extremely small (of the order 0.3µm) and the number of pore elements required to build a core-scale model that honours the true pore aspect ratio (radius/length) would run into the tens of millions. This means that only a portion of the full core composite can be realistically simulated without recourse to the scaling of certain fluid/rock parameters (although such a scaling approach will also be considered here alongside the true simulations to help give a fuller picture of the depletion process). Table 1 lists the network model dimensions.

2.5 Fluid and Rock/Fluid Properties

Having anchored the network model to the experimental composite, the supplied fluid properties and PVT data were then input into the simulator using appropriate pressure dependent functions as listed in Table 1. Representative average constant values of gas-water (σ_{GW}) and oil-water (σ_{OW}) interfacial tensions, $0.050\ N/m$ and $0.040\ N/m$, respectively, were estimated from the literature (Firoozabadi and Ramey, 1988). The associated spreading coefficient ($Cs = \sigma_{GW} - \sigma_{GO} - \sigma_{OW}$) suggests oil will be spreading in the presence of gas and water throughout depletion process. Representative values of

gas/oil and gas/water diffusion coefficients were also obtained from the literature (Zainal et al., 2009; Jamialahmadi et al., 2006; Lu et al., 2006; Bagrodia and Katz, 1977) and are given in Table 1 together with a general summary of the network and fluid properties.

The experimental depletion rate averages approximately 118 psi/day but was non-linear; fast at the beginning and slower towards the end. This non-linearity was captured in the model using a log function (Table 1). The pressure profile in the generic sensitivity and history matching runs followed this experimental profile. Subsequent *predictive* runs were performed at constant depletion rates.

Table 1: Summary of network and fluid properties for the 3D model

Initial Pressure, [psia]	3165
Final Pressure, [psia]	1000
Temperature, [^{o}F]	225
Gravity	Always on
Viscous Gradient	Negligible
Actual Core Height, [cm]	15.397
NX,NY,NZ	106,23,23
Model height, [cm]	0.25
Mean Radius, [μm]	0.23
R_{min}, R_{max}, [μm]	0.002, 0.389
Gas Molar Weight, [kg/mol]	0.0297
Gas Density at Std. Condition, [kg/m^3]	1.255824
Gas-Oil Diffusion Coefficient, [m^2/sec]	1.00E-8
Gas-Water Diffusion Coefficient, [m^2/sec]	1.00E-9
Gas-Water Interfacial Tension, [mN/m]	50.0
Oil-Water Interfacial Tension, [mN/m]	40.0
Gas-Oil Interfacial Tension, [mN/m]	= -6.014ln(P) + 50.227
Bo, oil formation volume factor	= 0.0001P + 1.1236
Bo, water formation volume factor	= -5E-06P + 1.0001
GOR, gas to oil ratio, [kg/m^3]	= 0.038P + 10.357
GWR, gas to water ratio, [kg/m^3]	= 0.0004P + 0.2363
ρ_{gas}, gas density, [kg/m^3]	= 0.06P - 7.73
ρ_{oil}, oil density, [kg/m^3]	= -0.0383P + 757.77
ρ_{water}, water density, [kg/m^3]	= 0.0002P + 998.65
μ_{gas}, gas viscosity, [PaS]	= 1E-08P + 5E-06
μ_{oil}, oil viscosity, [PaS]	= -4E-08P + 0.0004
μ_{water}, water viscosity, [PaS]	= 4E-20P + 0.0007
Experiment time varying pressure profile	= -854ln(t) + 9918.7
	Where, P = pressure in psia

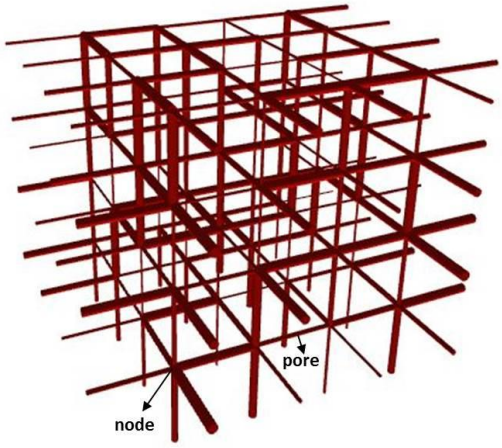

Figure 1: A three dimensional network model

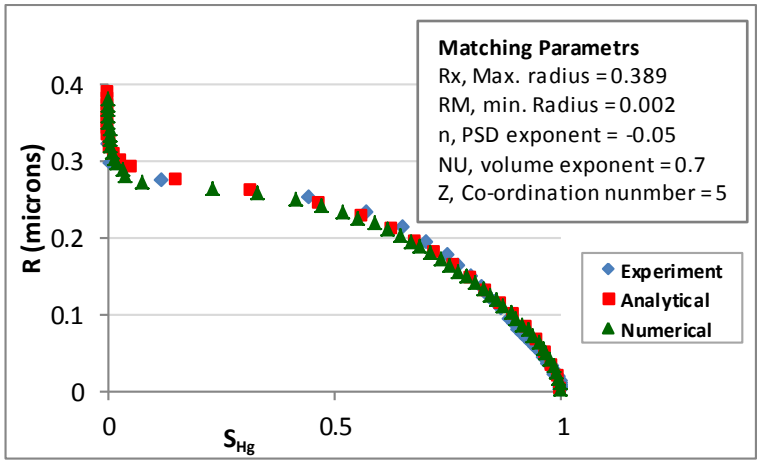

Figure 2: Matching radii vs. saturation (Mercury) plots to generate network anchoring parameters.

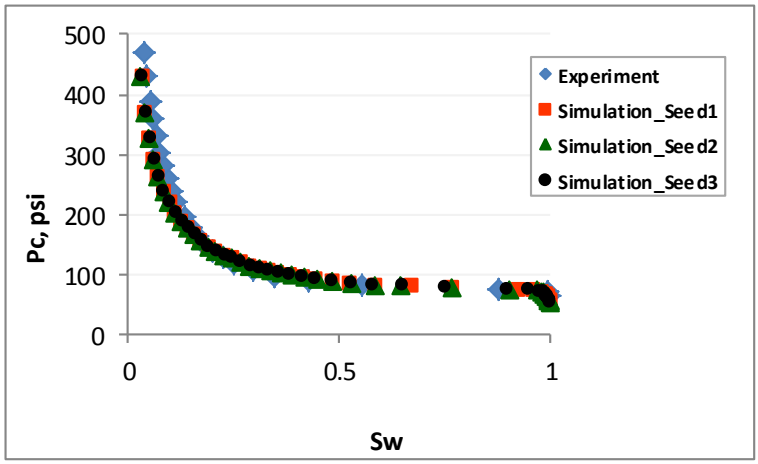

Figure 3: Comparison of experimental and numerically generated drainage Pc curves initialized at different random seeds.

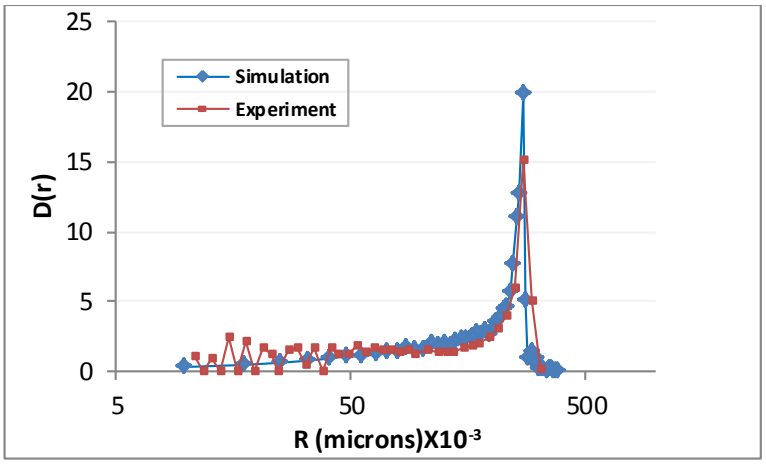

Figure 4: comparison of simulated and experimental plots of normalised "pore size distribution" vs. radius, demonstrating a uni-modal "pore size (actually, pore volume) distribution".

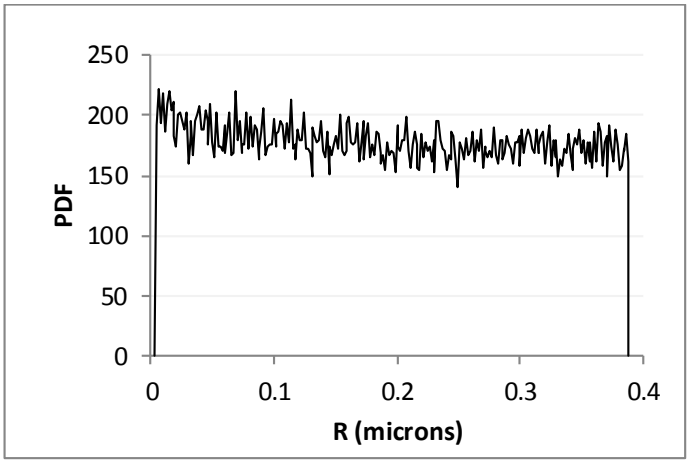

Figure 5: Probability density function vs. radius plot of simulation model, indicating a flat PSD.

3 Simulation of the Depletion Experiment

Figure 6 shows a sketch of the experimental set-up used for the Field A depletion, the two most important features being a core unit hydraulically connected to a separator. The core was charged with water and oil, occupying 0.616PV and 0.384PV respectively, while the separator was filled with oil of known quantity. From some pressure above the bubble point, the core pore pressure was gradually decreased below the bubble point down to 1000 psig. Gas was liberated during this process and the changes in fluid levels in the separator cell with pressure decline were recorded. To get an idea of the contribution of the core to the changes in separator fluid levels during depressurization, the separator unit was isolated and depressurized alone (starting with the same fluid level as in the whole system depressurization). The fluid levels recorded during the second process (cell only depressurization) were then compared to levels obtained from the whole system de pressurization and the difference inferred to originate from the core. At the end of whole system depressurization, the water saturation was found to be largely unchanged at 0.577PV, oil saturation decreased to 0.188PV and gas saturation stood at 0.230PV.

3.1 History Matching the Model

This is the culmination of the model calibration process that began with network anchoring, and hard-wiring of fluid and rock/fluid properties. History matching is the process of benchmarking the model to historical data.

For this case study, history matching involves searching for the appropriate progressive nucleation statistics of crevice size distribution and crevice density to produce the right number of bubbles that will match the experimental saturation profile. Equation (7) specifies the nucleation criteria.

The imbibition Pc curve from the core (Figure 7) suggests partial oil wetting. For modelling purposes we assumed a mixed-wet system where water and oil phase are randomly distributed in pores of all sizes.

The contact angle in Equation (7) was set at zero and a crevice size interval of $[1.0 \times 10^{-9}m, 20.0 \times 10^{-9}m]$ was assumed. Crevices were distributed uniformly across the network and sites were restricted to oil pores only, in line with other experimental observations that show nucleation to be most prevalent in the less wetting oleic phase (Mackay et al., 1998; Dominquez et al., 2000). Production of gas was allowed at the upper boundary of the network to mimic experimental boundary conditions.

Figure 8 shows crevice densities in the range 1/300 to 1/700 [crevice/$n_{oil\text{-}filled\ pores}$] have produced sufficient bubble nuclei for the model to match the experiment. Ultimately the 1/500 crevice density which yielded a total of 231 nuclei was selected for subsequent simulation runs. Figure 9 shows 3D phase saturation graphics at the end point of depletion simulations for 3 different nucleation densities. Since the model only spans a vertical dimension of 0.25cm it should therefore be noted that the gravitational force was scaled up by a factor of 61.56 so that networks used in these simulations (and those to be presented in the following section) correspond to physical samples that are 15.397cm in height i.e. the actual height of the core used in the experiment. A fuller discussion of this scale up technique will be presented later.

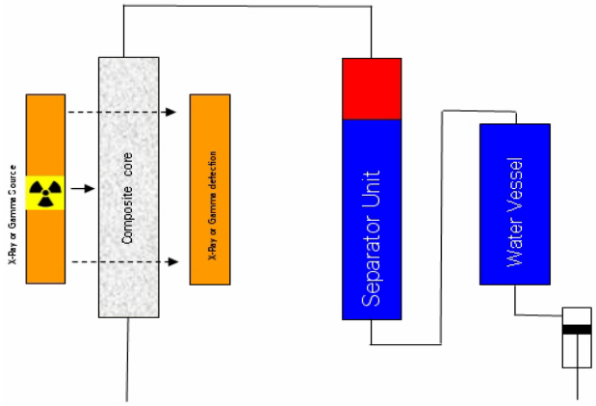

Figure 6: Schematic of the experimental set up

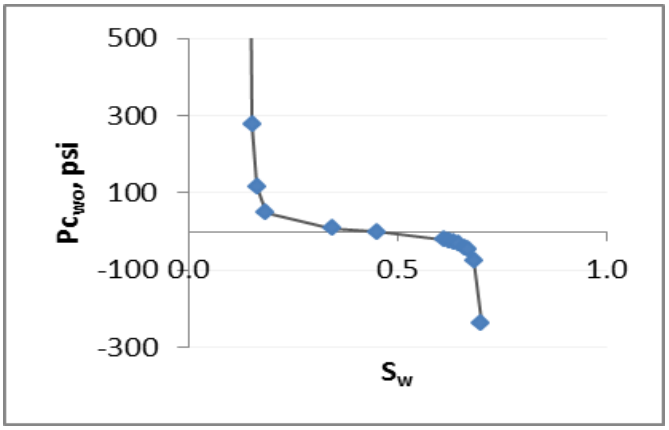

Figure 7 The experimental water-oil capillary imbibition curve

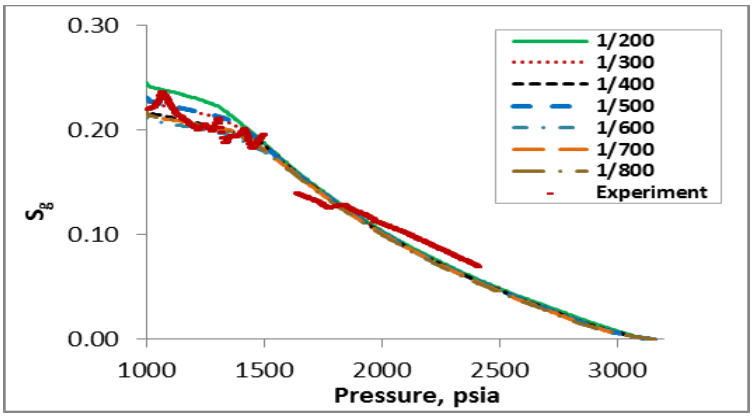

Figure 8: Finding a matching crevice density with progressive nucleation: Core gas saturation build-up at different crevice densities

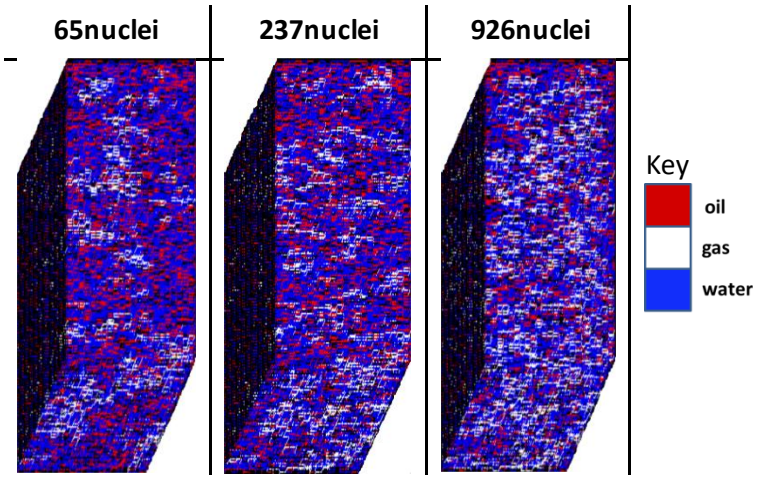

Figure 9: 3D mixed-wet waterflooded models: Fluid occupancy graphics at 1000psia for different nucleation densities.

4 Predictive Simulation Runs

Having now anchored our network model analogue to the Field A material, we next run a number of "what if" scenarios to derive correlations between important reservoir simulation parameters (critical gas saturation and relative permeability) and model variables such as initial water saturation, depletion rate, and core length.

4.1 Impact of Depletion Rate on Critical Gas Saturation (S_{gc})

Critical gas saturation is assumed to correspond to the saturation at which a sample spanning gas cluster is formed from the core inlet to the outlet (although discontinuous gas fluxes can occur under large gravitational and/or viscous pressure gradients). The spanning cluster definition seems appropriate here given the predominance of capillary forces and the relatively high nucleation densities expected during Field A depletion. A range of depletion rates (1.0psi/day – 200psi/day) was chosen to cover much of the observed range of values across a typical reservoir – from the near-well regions to the farthest reservoir boundaries.

Results

Experimental studies have repeatedly shown that nucleation density and critical gas saturation increase with an increase in depletion rate (Kennedy and Olson, 1952; Stewart et al., 1954; Berry, 1956; Handy, 1958; Moulu and Longeron, 1989; Kortekaas and Poelgeest, 1991; *inter alia*). It is therefore striking to see that in Figure 10A nucleation density changed only slightly as the depletion rate was varied over two orders of magnitude. However, two important features set apart the Field A

core (and by extension its numerical analogue) from the porous media used in the experiments cited above. All the porous media used in the referenced papers were not waterflooded and had permeabilities that range from 200mD to several Darcies (200mD for Stewart et al., 1954; 211mD for Moulu, 1989; 200 – 1900mD for Kortekaas and van Poelgeest, 1991; Micromodels for Bora et al., 2000; Bead packs for Chateneva et al., 1959; and Crystal surfaces for Kennedy and Olson, 1952). In contrast, the Field A core was (i), waterflooded, and (ii), has an average permeability of approximately 0.271mD.

Under virgin conditions and in high permeability media, diffusion occurs more rapidly and concentration gradients quickly flatten, lowering local supersaturation and hindering further nucleation. In waterflooded and tight media, however, there are fewer and narrower channels for diffusive mass transport and therefore considerably more time is required for the system to equilibrate. This leads to higher degrees of local supersaturation that increase the potential for bubble nucleation (see nucleation criteria in Equation (7). Unless depletion rates are set extremely low (less than 0.001psi/day, for example), ultra-low diffusion rates will suppress the effect of depletion rate on nucleation density in tight and waterflooded systems.

Figure 11 shows the predicted effect of depletion rate upon critical gas saturation in the Field A sample – the correlation between depletion rate and critical gas saturation can be seen to be very weak. Varying the depletion rate over two orders of magnitude changed the overall nucleation density by only 1.3% (232nuclei versus 229nuclei), and the critical gas saturation from 0.19 @ 200psi/day to 0.17 @ 10psi/day.

Results from other realisations using different random number seeds (used to define the error bars) predict that, on average, critical gas saturation should remain relatively constant (Scg ≈ 20%) for the Field A sample over the full range of depletion rates considered.

4.2 Impact of S_{wi} on S_{gc}

There are conflicting accounts of the effect of S_{wi} upon critical gas saturation in the depressurization literature. Whilst some authors (Kortekaas and Poelgeest, 1989) report that S_{gc} increases with S_{wi}, others (Moulu and Longeron, 1989; Firoozabadi et al., 1992), maintain that the opposite is true. In the face of these contrasting claims, pore network modelling can provide a means for examining these issues from first principles.

A fixed depletion rate of 5psi/day was chosen for the S_{wi} sensitivity study here and a number of simulations were performed at different initial water saturations –from Swi=0.0 to Swi=0.65.

Results

Figure 12A shows that nucleation density (in terms of the number of nuclei per initial oil volume) increases monotonically with increased S_{wi}. This, however, does not translate into a corresponding increase in S_{gc} as S_{wi} increases (Figure 12B). Indeed, S_{gc} is predicted to broadly *decline* with an increase in S_{wi} (S_{gc} decreases from 27% to 17% as S_{wi} is increased from 0% to 65%).

Two competing effects operate to modify S_{gc} as S_w is varied. Firstly, an increase in nucleation density (which generally increases S_{gc}) and secondly, a reduction in oil connectivity (which slows diffusional mass transport and reduces the probability of gas cluster coalescence). These two mechanisms tend to offset one another and only through simulation can we predict which will win out. The results (Figure 12) show an increase in S_{gc} as S_{wi} increased from 0.15 to 0.25, whilst further increase in S_{wi} above 0.25 leads to a progressive decrease in the bulk oil connectivity, choking off bubble coalescence and ultimately leading to an inverse correlation between S_{wi} and S_{gc}.

Although the relationship between S_{gc} and S_{wi} is nonlinear, oil recovery efficiency was predicted to increase as S_{wi} increased (Figure 13).

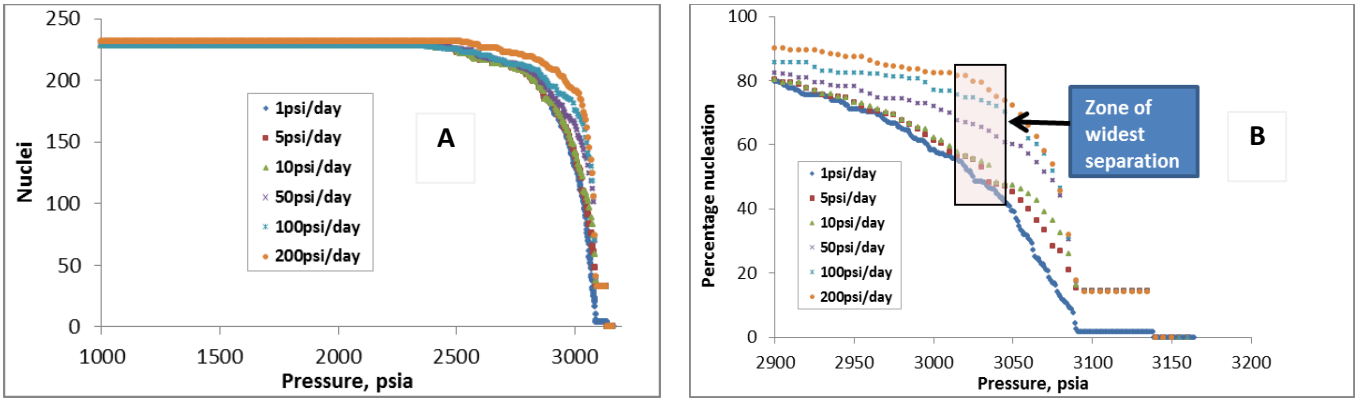

Figure 10:Impact of depletion rate on (A) Nucleation count, and (B) Differential nucleation rate in the early stages of depletion

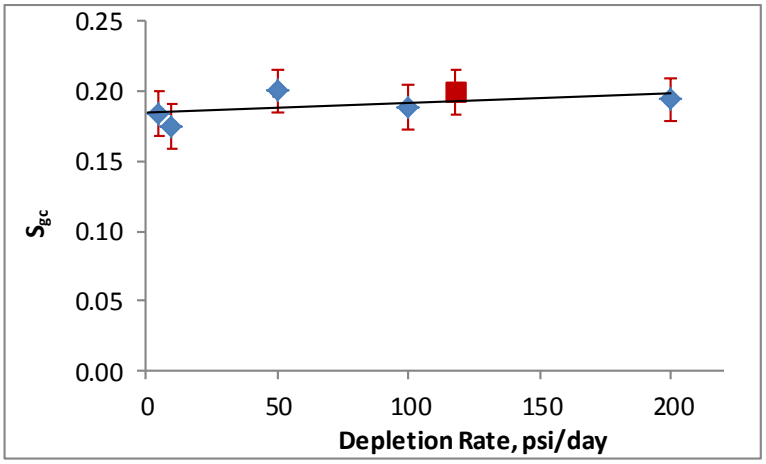

Figure 11: Correlation of critical gas saturation with depletion rate including uncertainty bars. Red square represents S_{gc} at the experimental rate (S_{wi}=0.616)

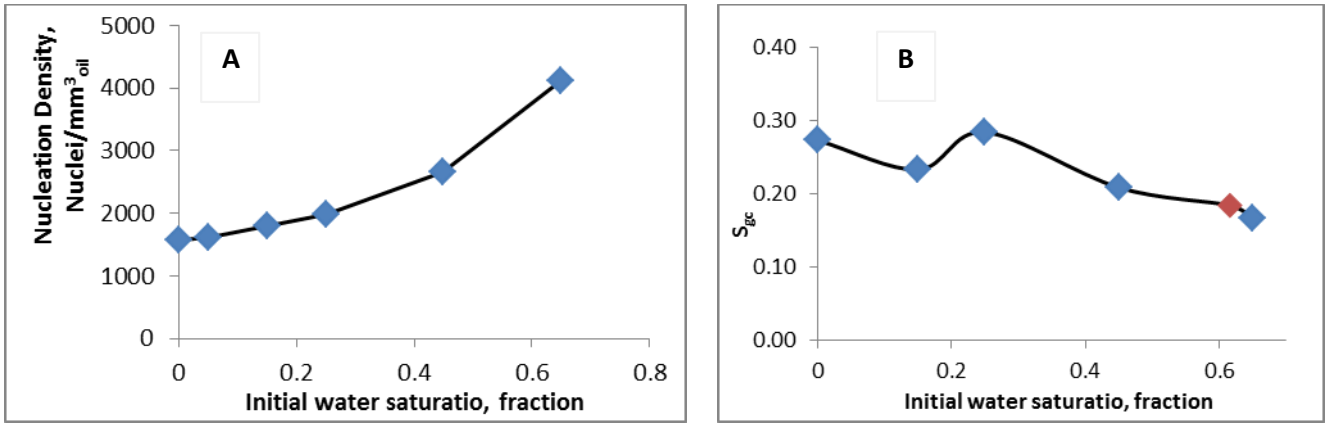

Figure 12: Impact of initial water saturation on (A) nucleation density, and (B) Critical gas saturation

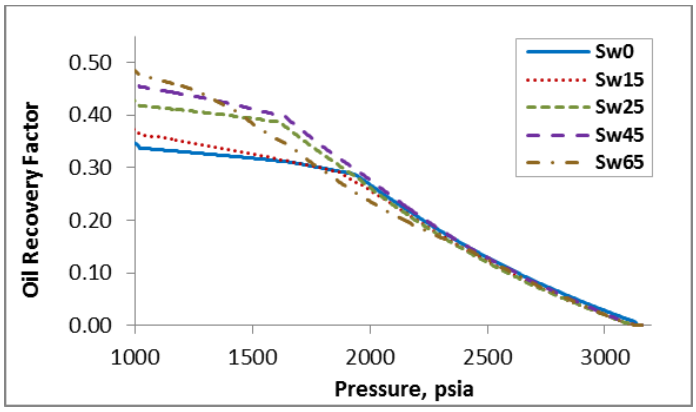

Figure 13: Cumulative oil recovery factor profiles at different S_{wi}.

4.3 Impact of Bond Number on S_{gc}

Whilst it is clearly impractical to build network models at the scale of several metres, it *is* possible to scale the capillary-gravitational force balance operating on the system by varying the local Bond Number – the relative importance of gravity and capillary forces affecting a gas cluster can be quantified through this dimensionless ratio, *viz*:

$$B_o = \frac{r\Delta\rho g h}{2\sigma} \qquad (19)$$

where $\Delta\rho$ is the density difference between oil and gas, σ the gas-oil interfacial tension, g the gravity constant, r the largest pore redius at the perimeter of the gas-oil interface, and h the vertical height of the evolving gas structure

Hence, the impact of system size on depletion behaviour can be inferred from simulations using a smaller network model, so long as the associated Bond Numbers are consistent. This can be achieved by, for example reducing interfacial tension and/or increasing the gravitational constant (g) in the small-scale simulations.

We choose to use the gravitational constant as the scaling parameter for the Bo by decreasing it through three orders of magnitude from the base case – equivalent to scaling the network model to represent different system heights. Hence: Bo = 0.01 ≡ 15.397cm; Bo = 0.05 ≡ 153.97cm; Bo = 0.54 ≡ 15.397m, Bo = 2.21 ≡ 153.97m (Note the representative Bo values here are averages computed over the course of the depletion process).

A high depletion rate (100 psi/day) was used to expedite these results. Note that we are using vertical 2D networks (213 X 47 X 1) here in order to consider larger networks – very large 3D networks are not feasible at present due to the small pore sizes associated with the low permeability Field A material. In order to construct 2D systems with relative diffusion surface area equivalent to that in the 3D network analogue, we have reduced the initial water saturation in the 2D model in proportion to the ratio of percolation thresholds characterising the 2D and 3D systems (i.e. such that Swi_2D= Pth_2D/Pth_3D * Swi_3D). Hence, the S_{wi} in the 2D model is 0.232 as against 0.616 in the 3D model.

Gravity impacts the depletion process in two fundamental ways: first, by biasing the activation of nucleation sites (a natural consequence of the increase in hydrostatic pressure that comes with an increase in system height); and secondly, by biasing the growth of nucleated bubbles. The simulations predict that gas saturation broadly decreases with an increase in Bond Number (or, equivalently, network height) – see Figure 14 and Figure 15, which plot maximum Bond Number and gas saturation profiles respectively. The effect of gravity growth bias can be seen at Bo = 0.54 – which is equivalent to increasing the height of the network to 1539.7cm. At Bo >= 2.21, spontaneous cluster migration can be

deduced from the Bo (Bond number) plot, although this is not obvious from the pore occupancy graphics in Figure 16. At Bo >= 2.21, nucleation became biased towards the top of the network accompanied by a clear transition in flow regime to a dispersive migratory regime (Bagudu et al., 2015). From the simulations *we see that S_{gc} is essentially scale-dependent* (see Figure 15(B)), which raises some important issues when attempting to populate reservoir-scale models. The results also suggest that *the impact of gravity on critical gas saturation should remain negligible in waterflooded Field A material up to a height of approximately 15m*.

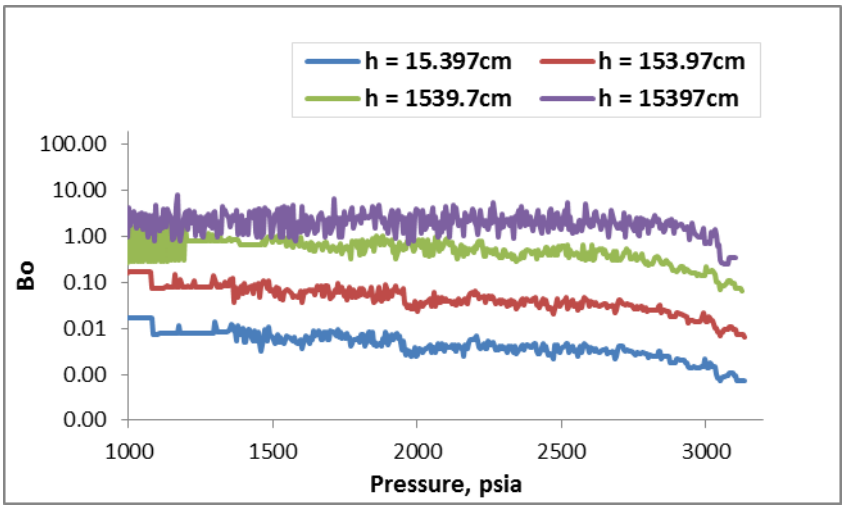

Figure 14: 2D Bomax (local maximum Bond number) profiles for different values of g at 100psi/day and S_{wi}=0.232.

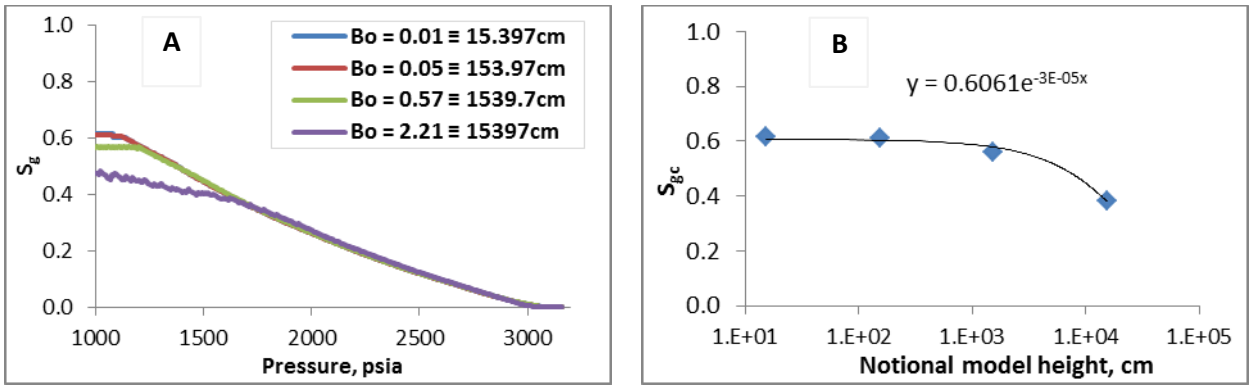

Figure 15: The impact of gravity constant (used as a scaling cipher) on (A) the S_g profile and (B) correlation of S_{gc} and network height, at 100psi/day and S_{wi}=0.232.

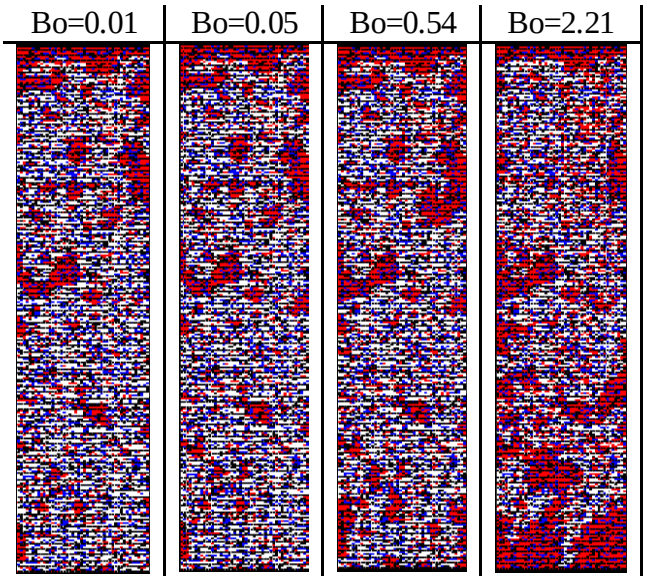

Figure 16: Pore occupancy graphics at 1000psia for varying *g* values at S_{wi}=0.232. Depletion rate was at 100psi/day.

4.4 Definition of S_{gc} and the Impact of Various System Parameters

Throughout this paper plots of gas evolution (and hence oil production) as functions of pressure have been presented. However, no explicit indication of how the critical gas saturation values have been estimated was given and the snapshots in Figure 16 suggest that we need to take care when defining this important parameter.

One definition corresponds to the saturation at which a continuous interconnected gas phase first spans the porous medium – and even this may be direction-dependent if the evolution regime is gravity-biased. Figure 15 and Figure 16 demonstrate the difficulty: the model with Bo = 2.21 has non-zero gas fluxes exiting the system, yet no spanning gas cluster emerge. Similarly, cases where fractures are important are likely to produce gas at very low critical saturations. So how can we infer S_{gc} from our simulations? We return to the 2D results for some insight.

Figure 17 presents plots of cumulative gas production (i.e. gas leaving the top of the system and immediately removed from the upper buffer) as functions of gas saturation within the entire network for different Bo (i.e. length scales). These plots exhibit asymptotic behaviour that is a useful diagnostic of critical gas. For Bo>=2.21, gas becomes increasingly more mobile and the flow becomes increasingly discontinuous – no spanning clusters form. For such migratory cases, S_{gc} may be better defined as the saturation at first production: this would give very low S_{gc} values that may even approach zero in some cases.

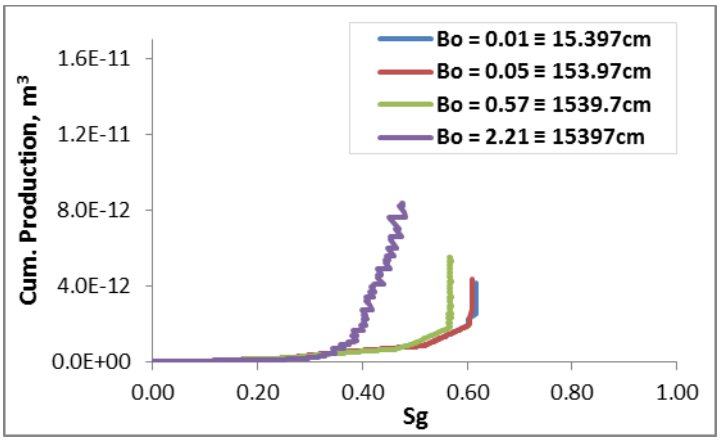

Figure 17: Estimation of 2D critical gas saturation using the cumulative gas production for varying model size. S_{wi}=0.232 and depletion rate at 100psi/day.

5 A generalized correlation function for S_{gc}

Simulations of the sensitivity of depletion behaviour to some key system parameters (S_{wi}, depletion rate, and system scale) have yielded single variable correlations with S_{gc}, each derived using base assumptions that may not necessarily correspond to the exact conditions in a given field. For example, the S_{gc} vs. S_{wi} correlation in Figure 12 was determined under the assumption of a depletion rate of 5 psi/day with a scaled height equivalent to that of the experimental core. Given that wide deviations from these assumed conditions are likely to occur, the S_{gc} vs. S_{wi} curve must be modified accordingly. A method for approximating S_{gc} under conditions when multiple variables are involved is described below and allows us to predict Sgc for different regions of a given reservoir from a single coreflood experiment in tandem with pore network modelling simulations.

For each single variable correlation of S_{gc}, a normalised equivalent is constructed using the conditions used in the experiment as a reference frame, as shown in Figure 18. Given any set of operating conditions (S_{wi}, depletion rate, system scale), an effective critical gas saturation $(S_{gc})_{Effective}$ can then be determined as follows:

1. Read off the corresponding normalised S_{gc} factors from the matching graphs in Figure 18
2. Use these factors to calculate the effective S_{gc} from the equation:

$$(S_{gc})_{Effective} = (S_{gc})_{Exp.} \times f_{DPrate} \times f_{Swi} \times f_{scale} \quad (20)$$

where, $(S_{gc})_{Exp.}$ is the S_{gc} obtained under experimental conditions

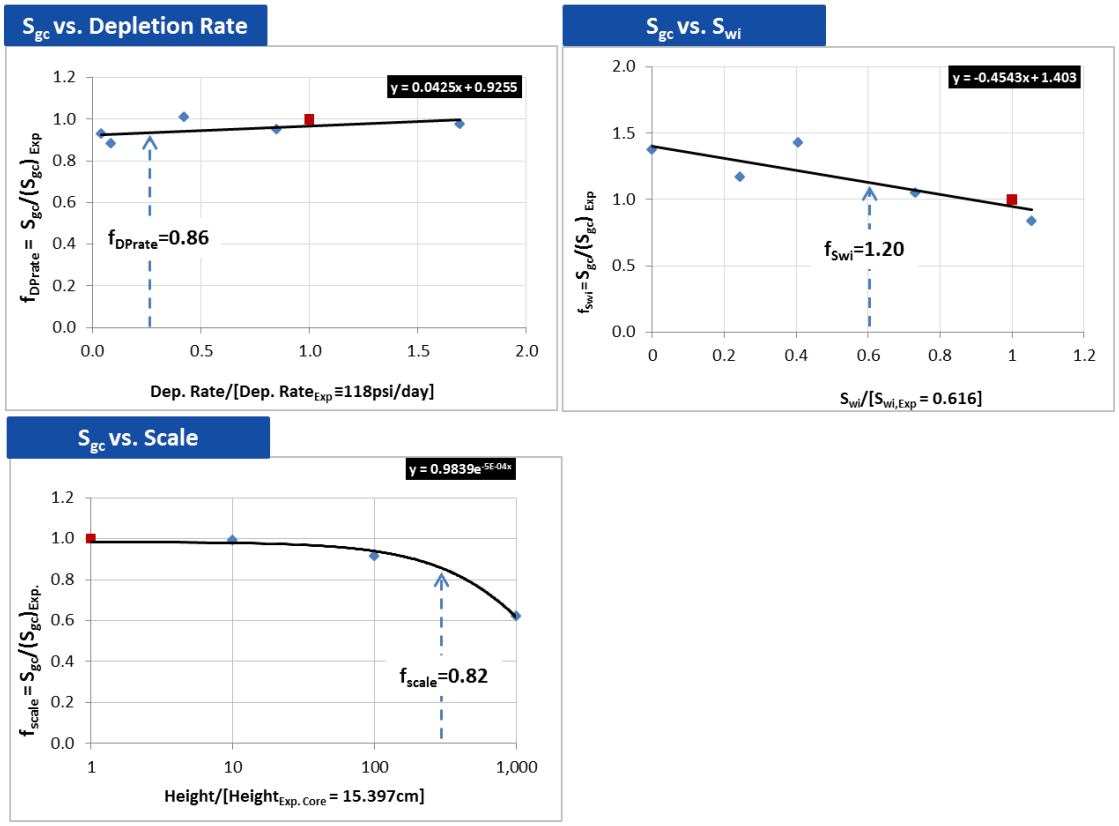

Figure 18: Normalised correlations of S_{gc} with some system variables. The red squares correspond to normalised experimental values. The S_{gc} factors displayed are examples.

6 Discussion of Results.

A number of variables related to rock and fluid properties, and a range of operational parameters impact the efficiency of a solution gas drive process. A widely use method for inferring the efficiency of solution gas from laboratory experiments is the measurement of the critical gas saturation. Values of S_{gc} reported based on experiments on reservoir core samples vary between 0.06 (Firoozabadi et al., 1992) to 0.27 (Madaoui, 1975) and the dependence of S_{gc} on depletion rate, interfacial tension, initial water saturation, oil viscosity, and system size have been extensively studied. While these efforts have yielded valuable insights into the nature of the individual mechanisms involved – bubble nucleation and growth, the nature of non-equilibrium mass transfer processes, etc, – there is as yet no unifying theory that unambiguously explains the results of the wide range of experimental observations reported in the literature.

Differences in data acquisition and interpretation techniques, and a general lack of clarity about the fundamental processes involved have often resulted in irreconcilable explanations of the same phenomena. Thus, there is a prevailing opinion that each depressurisation study is unique. We now attempt to place the Field A depletion behaviour in the context of other relevant published results of experimental depressurisation studies.

First, a brief recap of Field A's depletion characteristics: The Field A core has a permeability of 0.234mD and the minimum GOIFT for the fluid system was estimated at 1.8mN/m. The S_{gc} obtained by 3D network simulations using models anchored to the Field A sample ranged from 0.27 to 0.17 as S_{wi} was increased from 0 to 0.65. S_{gc} was relatively insensitive to changes in depletion rate from 200psi/day to 5psi/day but S_{gc} increased with decreasing S_{wi}.

Table 2 summarises a range of S_{gc} values obtained from depletion experiments on rock samples with absolute permeability, S_{wi}, and depletion rates in the ranges 0.04 – 2060mD, 0 – 0.73, and 0.44 – 172800psi/day, respectively.

Table 2: Summary of selected depressurization data from literature

Authors	Year	K, mD	S_{gc}, fraction	DP Rate, psi/day	S_{gc} vs. DP Rate	S_{wi}, fraction
Petersen et al. (Brent Group, Statfjord Field)	2004	990	0.064 – 0.122	115 - 731	increase with	0.179 - 0.619
Petersen et al. (Brent Group, Statfjord Field)	2004	711	0.084 – 0.134	115 - 731	increase with	0.173 - 0.731
Drummond (South Brae Field - North Sea)	2001	292	0.025	99	-	0.23
Egermann and Vizika	2001	3.2	0.24	2304	-	0.55
Naylor et al. (Miller Field)	2001	27	0.21	765	-	0.52
Naylor et al. (Miller Field)	2001	492.5	0.06 – 0.16	89 - 26	increase with	0.70 - 0.73
Sahni et al.	2001	2000, 2060	0.06 – 0.11		increase with	0.0213
Kumar et al.	2000	1250, 1180	0.03 - 0.07		increase with	
Kamath and Boyer	1995	0.1	0.10	20	non-monotonic	
Kamath and Boyer	1995	0.04	0.10	20 - 100	non-monotonic	0
Firoozabadi et al. (Berea)	1992	605	0.011 - 0.02		increase with	0
Firoozabadi et al. (Chalk)	1992	2.7	0.006 – 0.012		increase with	0
Kortekaas and van Poelgeest (Brent)	1991	230 - 1900	0.04 – 0.08	10 - 230	increase with	Virgin – watered out
Kortekaas and van Poelgeest (Brent)	1991	200 - 1100	0.07 – 0.10	10 - 230	increase with	Virgin – watered out
Moulu (St Maximin limestone)	1989	211.10	0.066 – 0.12	0.44 – 72.5	increase with	
Madaoui	1975		0.044 – 0.264	0.78 to 170	Non-monotonic	
Handy	1958	7.41	0.05 – 0.16	377 - 172800	increase with	

6.1 Impact of Capillary Radius or Permeability

The correlation between S_{gc} and permeability has not been firmly established and some authors (Kortekaas and van Poelgeest, 1991) have thrown serious doubt on whether such a correlation exists at all. However, in Table 2, and except for the data of Firoozabadi et al. (1992), the high S_{gc} values tend to correspond to cores with the lowest permeability, although in a somewhat non-linear way. This initial assessment, however, does not account for the effect of depletion rate (which differs from case to case). One of the highest S_{gc} values recorded in Table 2 (i.e. 0.24) was derived from a 3.2mD Palatinat sandstone core. This apparent trend is in line with our interpretation of the relatively high Field A S_{gc} values, which suggests that the small average pore radius led to rapid nucleation of embryonic bubbles and a highly dendritic bubble growth pattern largely unbiased by gravity.

6.2 Impact of Depletion Rate

An increase in depletion rate is generally known to increase bubble density which will in turn le ad to an increase in S_{gc}. However, the data of Kamath and Boyer (1995) and that of Madaoui (1975) in Table 2 showed otherwise. For the two Colton sandstone cores used by Kamath and Boyer (1995), increasing the depletion rate from 20psi/day to 100psi/day had no effect on S_{gc}. It is interesting that both Colton sandstone cores have permeabilities of a similar order of magnitude as the Field A core (the cores are in fact less permeable than the Field A core). The results of Kamath and Boyer (1995) support the conclusion that tight cores may require much longer time scales for equilibration to occur and this means that extremely low depletion rates are needed to reduce the S_{gc} from the values achieved at

typical laboratory depletion rates – a behaviour that has been repeatedly observed with respect to the Field A core.

6.3 Impact of S_{wi}

Data on the impact of S_{wi} on S_{gc} do not show a clear trend. Kortekaas and van Poelgeest (1991) reported a doubling of critical gas saturation from < 0.04 to 0.05 – 0.08 as S_{wi} was changed from virgin to watered-out conditions for three sandstone core samples (230mD, 550mD, and 1900mD) obtained from a Brent Group reservoir, while for two other samples (200mD and 1100mD, obtained from another Brent Group reservoir) an increase in S_{wi} had a negligible effect on S_{gc} – stabilising between 0.07 and 0.10 for virgin and watered-out samples. The differences in the trends of S_{wi} and S_{gc} between the two reservoirs were assumed to result from the differences in the mineralogical and morphological properties of the reservoir rocks. The two reservoirs were shown to have quite different clay structures, with one reservoir containing kaolinite-like sharp-edged booklets which could form preferred sites for bubble nucleation. The data of Peterson et al. (2004) showed a consistent decrease in S_{gc} as S_{wi} increased over a range of depletion rates for two core samples (990mD and 711mD) obtained from the Statfjord field in the North Sea. With respect to the Field A behaviour, while the S_{gc} decreased gradually as S_{wi} was increased, both nucleation density and the oil recovery efficiency increased as S_{wi} increased.

7 Conclusions

We have presented an analysis of a depressurization experiment carried out on a waterflooded North Sea reservoir core which demonstrates the power of the pore network modelling approach for sensitivity studies in complex experimental settings. The goal was to better characterize the uncertainties associated with the determination of S_{gc} and relative permeabilities under changing operating conditions. Additionally, a literature survey was presented that discussed the Field A results in the context of other published depressurisation experiments, particularly those conducted with samples from North Sea reservoirs.

The main conclusions are as follows:

- Decreasing depletion rate through three orders of magnitudes 100psi/day to 1psi/day did not have a significant effect on gas evolution and S_{gc}, regardless of S_{wi}. Results from several realizations, using different random seeds predict that critical gas saturation is effectively constant ($S_{gc} \approx 20\%$ at S_{wi} of 0.616) for the Field A sample over the full range of depletion rates considered. The two most plausible reasons for this behaviour are: (a) the extremely low equilibration rates imposed by the small pore sizes, and (b) the high bubble density facilitated by the low GOIFT at initial conditions.

- Nucleation density increased monotonically as S_{wi} increased: large S_{wi} effectively restricted diffusive mass transport, increased the local supersaturation and led to even higher nucleation densities. This, however, did not simply translate into a corresponding increase in S_{gc} as S_{wi} was increased. S_{gc} broadly declined with an increase in S_{wi} (S_{gc} varied from 0.27 – 0.17 as S_{wi} was increased from 0 to 0.65). Although critical gas saturation was found to be lower at larger values of S_{wi}, the oil recovery factor at the end of depletion increased with S_{wi}. Hence, depressurization as a recovery mechanism in chalk was predicted to approach its full potential in highly waterflooded systems.

- Gas saturation at any given pressure was found to broadly decrease with an increase in Bond Number (or, equivalently, network height). Thus S_{gc} was effectively scale-dependent, which raises some important issues when attempting to populate reservoir-scale models.

Nevertheless, simulation results suggest that the impact of gravity on critical gas saturation should remain negligible in waterflooded Field A material up to a height of approximately 15m.

- A generalised correlation function has been developed which can be used to estimate S_{gc} in chalk depressurisation for a wide range of operating conditions.

- In comparison to the surveyed published data on North Sea rocks that have been used in depressurization experiments, the properties of the Field A core are unique. While the Field A core has a permeability of about 0.23mD, the permeability of North Sea rocks used in reported depressurization experiments ranged between 27mD (from the Miller field – Naylor et al., 2001) and 1900mD (from the Brent reservoir – Kortekaas and van Poelgeest, 1991). With a few exceptions, the highest literature S_{gc} values corresponded to the lowest permeability rocks. An apparent insensitivity of the depressurization process to changes in depletion rate was also reported for these tight rocks (Kamath and Boyer, 1995; Madaoui, 1975). All evidence so far indicates that, given the pore microstructure, the instantaneous bubble nucleation mechanism, and the negligible impact of depletion rate on the Field A depressurization process, the high S_{gc} observed for Field A (averaging 0.20 for an S_{wi} of 0.61) was not particularly exceptional and similar examples could be found in the literature.

- The limit on the available CPU power had meant that we were unable to simulate large 3D networks without recourse to topological and scaling arguments. For the same reason, we have also only been able consider depletion rates down to 1psi/day. It is hoped that future improvements to the model will include increased computational efficiency to enable simulation of larger cores and depletion rates as low as 0.1 psi/day.

Acknowledgement

The authors gratefully acknowledge Peter Salino,. Gerald Hamon, and Igor Bondino for past discussions of issues associated with this study and Foundation CMG for funding the studentship for Usman Bagudu.

8 References

- Akin, S. and Kovscek, A.R.: "Heavy-oil solution gas drive: a laboratory study", Journal of Petroleum Engineering, vol. 35, pp. 33-48, 2002.

- Alshmakhy, A. and Maini, B.: "Effects of Gravity and Pressure Draw Down on Primary Depletion Recovery Factor in Heavy Oil Systems", proceedings, presented at the 2012 SPE Heavy Oil Conference, Calgary, Alberta, Canada, SPE 157821, 2012.

- Bagudu, U.: Pore Network Modelling of Gas Flow Processes in Porous Media with Special Application to CO2 Sequestration, PhD Thesis, 2015

- Bagudu, U., McDougall, S.R. and Mackay, E.J.: "Pore-to-Core-Scale Network Modelling of CO2 Migration in Porous Media", Transp Porous Media, 110:41–79, August, 2015.

- Bondino, I., Hamon, G., Kallel, W. and Kachuma, D.: "Relative Permeabilities from Simulation in 3D Rock Models and Equivalent Pore Networks: Critical Review and Way Forward", proceedings, presented at the SCA 2012 Symposium, Aberdeen, Scotland, UK, paper SCA2012-01, 2012.

- Boge, R., Lien, S., Gjesdal.A. and Hansen, A.: "Turning a North Sea Oil Giant Into A Gas Field - Depressurization of the Statfjord Field" SPE 96403, 2005

- Bondino, I., McDougall, S.R. and Hamon, G.: "Interpretation of a long-core heavy oil depletion experiment using pore network modelling techniques", proceedings, presented at the SCA 2003 Symposium, Pau, France, paper SCA2003-11, 2003.

- Bondino, I., Hamon, G., Kallel, W. and Kachuma, D.: "Relative Permeabilities from Simulation in 3D Rock Models and Equivalent Pore Networks: Critical Review and Way Forward", proceedings, presented at the SCA 2012 Symposium, Aberdeen, Scotland, UK, paper SCA2012-01, 2012.

- Bondino, I., McDougall, S.R. and Hamon, G.: "A pore-scale modelling approach to the interpretation of heavy oil pressure depletion experiments", Journal of Petroleum Science and Engineering, 65, pp. 14-22, 2009.

- Bora, R., Maini, B.B. and Chakma, A.: "Flow visualization studies of solution gas drive process in heavy oil reservoirs with a glass micromodel", SPE Reservoir Evaluation and Engineering, vol. 3 (3), pp. 224-229, 2000.

- Bratvold, R. B. and Thomas, P.: "A Real Options Approach to the Gas Blowdown Decision", SPE-174868, 2015.

- Drummond, A., Fishlock, T., Naylor, P. and Rothkopf, B.: "An evaluation of post-waterflood depressurization of the South Brae Field, North Sea", proceedings, presented at the 2001 SPE Annual Technical Conference and Exhibition, New Orleans, Louisiana, U.S.A., SPE 71487, 2001.

- Dumore' J.M.: "Development of gas-saturation during solution-gas drive in an oil layer below a gas cap", SPE Journal, pp. 211-218, 1970.

- Egermann, P. and Vizika, O.: "A new method to determine critical gas saturation and relative permeability during depressurization in the near-wellbore region", proceedings, presented at the SCA Symposium, Abu Dhabi, paper SCA2000-36, 2001.

- El Yousfi, A., Zarcone, C. and Bories, S.: "Physical mechanisms for bubble growth during solution gas drive", proceedings, presented at the SPE Annual Technical Conference and Exhibition, San Antonio, Texas, U.S.A., SPE 38921, 1997.

- Ezeuko, C.: "Network Modelling Studies of Depressurisation and Repressurisation Processes in Porous Media", PhD Thesis, Institute of Petroleum Engineering, Heriot-Watt University, 2009.

- Firoozabadi, A. and Kashchiev, D.: "Pressure and volume evolution during gas phase formation in solution gas drive process", SPE Journal, vol. 1, pp. 219-227, 1996.

- Firoozabadi, A. and Ramey, H.J.: "Surface tension of water-hydrocarbon systems at reservoir conditions", Journal of Canadian Petroleum Technology, vol. 27, pp. 41-48, 1988.

- Firoozabadi, A., Ottesen, B. and Mikkelsen, M.: "Measurements of supersaturation and critical gas saturation", SPE Formation Evaluation, pp. 337-344, December 1992.

- Goodfield, M. and Goodyear, S.G.: "Relative permeabilities for post-waterflood depressurization", proceedings, presented at the Offshore Europe 2003, Aberdeen, UK, SPE 83958, 2003.

- Handy, L.L.: "A laboratory study of oil recovery by solution gas drive", Petroleum Transactions, AIME, vol. 213, pp. 310-315, 1958.

- Kamath, J. and Boyer, R.E.: "Critical gas saturation and supersaturation in low permeability rocks", SPE Formation Evaluation, pp. 247-253, December 1995.

- Kennedy, H.T. and Olson, R.: “Bubble formation in supersaturated hydrocarbon mixtures”, Petroleum Transactions, AIME, vol. 195, pp. 271-278, 1952.

- Kortekaas, T.F.M. and van Poelgeest, F.: “Liberation of solution gas during pressure depletion of virgin and watered-out reservoirs”, SPE Reservoir Evaluation and Engineering, pp. 329-335, August 1991.

- Kumar, R., Pooladi-Darvish, M. and Okazawa, T.: “An investigation into enhanced recovery under solution gas drive in heavy oil reservoirs”, proceeding, presented at the 2000 SPE/DOE Improved Oil Symposium, Tulsa, Oklahoma, U.S.A., SPE 59336, 2000.

- Lago, M., Huerta, M. and Gomes, R.: “Visualization study during depletion experiments of Venezuelan heavy oils using glass micromodels”, Journal of Canadian Petroleum Technology, vol. 41 (1), Jan 2002.

- Lenormand, R. and Zarcone, C.: “Role of roughness and edges during imbibition in square capillaries”, proceeding, presented at the SPE Annual Technical Conference and Exhibition, Houston, Texas, U.S.A., SPE 13264, 1984.

- Li, X. and Yortsos, Y.C.: “Critical gas saturation: modeling and sensitivity studies”, proceedings, presented at the 68th Annual Technical Conference and Exhibition of the Society of Petroleum Engineers, Houston, Texas, U.S.A., SPE 26662, 1993.

- Ligthelm, D.J., Reijnen, G.C.A.M., Wit, K., Weisenborn, A.J. and Scherpenisse, D.J.: “Critical gas saturation during depressurization and its importance in the Brent Field”, proceedings, presented at the SPE 69th Annual Technical Conference and Exhibition, New Orleans, Louisiana, U.S.A., SPE 28475, 1997.

- Mackay, E.J., Henderson, G.D., Tehrani, D.H. and Danesh, A.: “The importance of interfacial tension on fluid distribution during depressurization”, SPE Reservoir Evaluation and Engineering, pp. 408-415, October 1998.

- Madaoui, K.: "Critical Gas Saturation in Depletion Drive," Reports of IntI. Symposium on Hydrocarbon Exploration, Drilling and Production Techniques 203, Dec. 10-12, 1975.

- McDougall, S.R. and Mackay, E.J.: “The impact of pressure-dependent interfacial tension and buoyancy forces upon pressure depletion in virgin hydrocarbon reservoirs”, Transactions IchemE, vol. 76, part A, pp. 553-561, 1998.

- McDougall, S.R. and Sorbie K.S.: “The missing link between pore-scale anchoring and pore-scale prediction”, proceedings, presented at the SCA 2002 Symposium, Monterey, California, U.S.A., paper SCA2002-25, 2002.

- McDougall, S. R., Cruickshank, J., & Sorbie, K. S. (2002). Anchoring methodologies for pore-scale network models: Application to relative permeability and capillary pressure prediction. Petrophysics, 43(4), 365-375.

- Moulu, J.C.: “Solution-gas drive: experiments and simulation”, Journal of Petroleum Science and Engineering,2, Pp379-386, 1989.

- Moulu, J.C. and Longeron D.: “Solution-gas drive: experiments and simulation”, proceedings, presented at the 5th European Symposium on Improved Oil Recovery, Budapest, 1989.

- Naylor, P., Fishlock, T., Mogford, D. and Smith, R.: “Relative permeability measurements for post-waterflooded depressurisation of the Miller Field, North Sea”, SPE Reservoir Engineering, 4(4), pp. 276-280, 2001.

- Nejad, K. S. and Danesh, A.: “Visual Investigation of Oil Depressurisation in Pores with Different Wettability Characteristics and Saturation Histories”, proceedings, presented at 2005 SPE Europec/EAGE Annual Conference, Madrid, Spain, paper SPE 94054, 2005.

- Petersen, Jr, E.B., Agaev, G.S., Palatnik, B., Ringen, J.K., Øren, P.E. and Vatne, K.O.: “Determination of critical gas saturation and relative permeabilities relevant to the depressurization of the Statfjord Field”, proceedings, presented at the SCA 2004 Symposium, Abu Dhabi, paper SCA2004-33, 2004.

- Piccavet, N., Long, J., Hamon, G., Bondino, I. and McDougall, S.: “Depletion of Near-Critical Oils: Comparison Between Pore Network Model Predictions and Experimental Results”, proceedings, presented at the SCA 2006 Symposium, Trondheim, Norway, paper SCA2006-32, 2006.

- Ritter, L. C. and Drake, R. L., "Macropore Size Distributions in Some Typical Porous Substanes", Ind. Eng. Chem. An. Ed. 17, 782 (1945).

- Sahni, A., Gadelle, F., Kumar, M., Tomutsa, L. and Kovscek, A.R.: “Experiments and analysis of heavy-oil solution-gas drive”, proceeding presented at SPE Annual Technical Conference and Exhibition, New Orleans, U.S.A., SPE71498, 2001.

- Scherpenisse, W., Wit, K., Zweers, A.E., Shoei, G. and van Wolfswinkel, A.: “Predicting Gas Saturation Buildup During Depressurisation of a North Sea Oil Reservoir”, proceedings, presented at the European Petroleum Conference, London, U.K., SPE 28842, 1994.

- Sorbie, K. S. and Skauge, A.: “Can Network Modelling Predict Two-Phase Functions”, proceedings, presented at the SCA 2011 Symposium, Austin, Texas, U.S.A., SCA2011-29, 2011.

- Stewart, C.R., Hunt, E.B., Schneider, F.N., Geffen, T.M. and Berry, V.J.: “The role of bubble formation in oil recovery by solution gas drive in limestones”, Petroleum Transactions, AIME, vol 201, pp. 294-301, 1954.

- Tsimpanogiannis, I.N. and Yortsos, Y.Y.: “Model for the gas evolution in a porous medium driven by solute diffusion”, AIChE Journal, vol. 48 (11), pp. 2691-2710, 2002.

- Zainal, S., Yee, H. V., Saaid, I. M. and Jelani, J.: “An Evaluation of Gas Diffusivity Measurement in Reservoir Fluid from Low to High Pressure Systems for Oil Recovery Applications”, proceedings, presented at International Petroleum Technology Conference, Doha, Qatar, &-9 December 2009.